Performance Analysis of Masdar City's Concentrated Solar Beam-Down Optical Experiment

Marwan Mokhtar
Research Engineer
Laboratory for Energy and Nano Science (LENS)
Department of Mechanical Engineering
Masdar Institute of Science and Technology
Abu Dhabi, UAE
Email: marwan.mukhtar@gmail.com

Steven A. Meyers
Research Engineer
Laboratory for Energy and Nano Science (LENS)
Department of Mechanical Engineering
Masdar Institute of Science and Technology
Abu Dhabi, UAE

Peter R. Armstrong
Associate Professor
Laboratory for Energy and Nano Science (LENS)
Department of Mechanical Engineering
Masdar Institute of Science and Technology
Abu Dhabi, UAE

Matteo Chiesa
Associate Professor
Laboratory for Energy and Nano Science (LENS)
Department of Mechanical Engineering
Masdar Institute of Science and Technology
Abu Dhabi, UAE

An analysis of the Beam Down Optical Experiment (BDOE) performance with full concentration is presented. The analysis is based on radiation flux distribution data taken on 21st March 2011 using an optical-thermal flux measurement system. A hypothetical thermal receiver design is used in conjunction with the experimental data to determine the optimal receiver aperture size as a function of receiver losses and flux distribution. The overall output of the plant is calculated for various operating temperatures and three different control strategies namely, constant mass flow of the Heat Transfer Fluid (HTF), constant outlet fluid temperature and real-time optimal outlet fluid temperature. It was found that the optimal receiver aperture size of the receiver ranged between (1.06 and 1.27 m^2) depending on temperature. The optical efficiency of the BDOE ranged between 32% to 37% as a daily average. Depending on the control parameters and assuming an open receiver with solar absorptivity of 0.95 and longwave emissivity of 0.10, the average receiver efficiency varied from 71% at 300^{o}C down to 68% at 600^{o}C. The overall daily average thermal efficiency of the plant was between 28% and 24% respectively for the aforementioned temperatures. The peak of useful power collected in the HTF

was around 105 kW_{th} at 300^{o}C mean fluid temperature and peaked around 89 kW_{th} at 600^{o}C.

Nomenclature

α Receiver absorptivity in solar spectrum
β Volumetric thermal expansion coefficient (K^{-1})
γ Receiver intercept factor
ΔT Temperature difference between mean plate temperature and ambient air temperature (K)
ε Receiver longwave emissivity
ν Kinematic viscosity of air (m^2/s)
σ Stefan-Boltzmann constant ($5.670373x10^{-8}Wm^{-2}K^{-4}$)
A Receiver aperture area (m^2)
C_p Specific heat of the HTF at constant pressure ($kJkg^{-1}K^{-1}$)
D_i Receiver inner tube diameter (m)
D_o Receiver outer tube diameter (m)
F' Receiver efficiency factor
F_R Heat removal factor
g Gravitational acceleration (m/s^2)
Gr Grashof number
$G(r,\theta)$ Radiation flux map in polar coordinates (kW/m^2)
$\bar{h}_c$ Receiver convection heat transfer coefficient ($kWm^{-2}K^{-1}$)
h_f Convection heat transfer coefficient between HTF and tube wall ($kWm^{-2}K^{-1}$)
$\bar{h}_r$ Receiver linearized radiative heat transfer coefficient ($kWm^{-2}K^{-1}$)
k Thermal conductivity of air ($Wm^{-1}K^{-1}$)
L Receiver characteristic length (m)
$\dot{m}$ HTF mass flow rate (kg/s)
Nu Nusselt number
Pr Prandtl number
$\dot{q}_{in}$ Solar flux intercepted by the receiver (kW/m^2)
$\dot{Q}_{rad}$ Radiative heat loss (kW)
$\dot{Q}_u$ Useful thermal power (kW)
R Receiver aperture radius (m)
Re Reynolds number
T_e Ambient air temperature (^oC)
T_{fi} Inlet mean fluid temperature (^oC)
T_{film} Mean film temperature (^oC)
T_{fo} Outlet mean fluid temperature (^oC)
T_{opt} Real-time optimized fluid outlet mean temperature (^oC)
T_{mp} Mean plate temperature (^oC)
T_{sky} Effective sky temperature (^oC)
U_L Overall heat loss coefficient ($kWm^{-2}K^{-1}$)

Abbreviations

BDOE Beam-Down Optical Experiment
CCD Charge-Coupled Device
CR Central Reflector
CSP Concentrated Solar Power
DNI Direct Normal Irradiation
HFS Heat Flux Sensor
HTF Heat Transfer Fluid
LEC Levelized Energy Cost

1 Introduction

Central receiver Concentrated Solar Power (CSP) plants promise higher energy conversion efficiency and consequently lower levelized energy cost (LEC) [1]. It is expected that 48% of the cost reduction in tower plants costs will come from technology research and development [2]. The beam down concept has the potential of producing energy at lower costs due to the ability of locating bulky receivers on ground level in addition to the possibility of using smaller receiver apertures and secondary concentrators which is made possible by the narrower view angle of concentrated radiation [3]. In order to demonstrate the potential of such configuration and investigate the possibility of a scale-up, a pilot 100kW$_{th}$ Beam-Down Optical Experiment (BDOE) was constructed in 2009 in Masdar City Abu Dhabi (24.44^{o}N 54.61^{o}E), see Fig. 1.
The heliostat field consists of 33 ganged-type heliostats of totaling 280 m^2 of reflective area (see [4] for more details). In this paper we present optical and thermal performance analysis of BDOE based on experimental data collected in March 2011.

Optical performance is quantified by the optical efficiency, which includes the effects of cosine loss, reflectivity loss, beam attenuation loss, blocking and shading loss in addition to light spillage around central reflector (CR) mirrors and around the receiver aperture (intercept factor).The combined effect of the aforementioned (except for the final intercept factor) is evaluated experimentally using the flux measurement system. The intercept factor is a function of receiver aperture size/geometry and flux distribution. Consequently, the receiver aperture size must be specified in order to evaluate the optical efficiency.

Thermal performance depends on the thermal efficiency of the receiver, which, similar to optical efficiency, is also a function of receiver aperture size/geometry. Thermal performance is also clearly dependent on the operating temperature.
Because of the inverse effects of receiver size on optical and thermal efficiency, an optimization is necessary to determine size and operating temperature to maximize a certain objective function. The objective function used in our case is total daily energy collection.

2 Experimental Setup

To study energy flux distribution and its magnitude on the focal plane of the BDOE, concentrated solar radiation is intercepted by a 5m x 5m ceramic tile target, located 2.3m above ground level (see Fig. 1). These white tiles can withstand the high flux levels and are highly reflective in a diffuse manner approximating a Lambertian target. This allows a CCD camera located at the top of the tower to measure the distribution of luminous intensity. Embedded within the tiles at eight locations are heat flux sensors (HFS) to measure the concentrated solar flux. The HFSs only provide discrete thermal flux data and the CCD camera provides data of

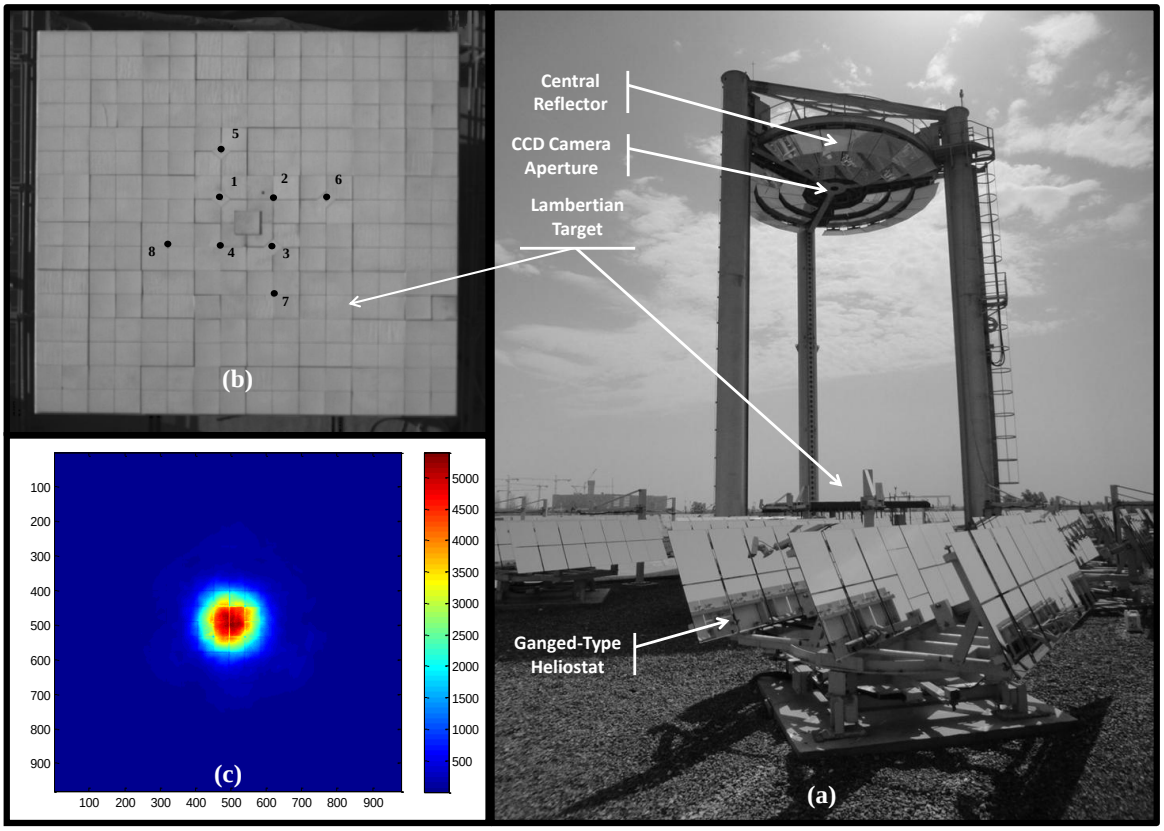

Fig. 1. BDOE Overview. (a) Ganged-Type heliostat field and central reflector mirrors. CCD camera aperture is in the center of the central reflector taking shots of the Lambertian target below it. (b) Embedded within the Lambertian target are water-cooled heat flux sensors at eight locations to calibrate the CCD camera images. (c) A typical luminance map taken by the CCD camera.

the luminous intensity on the target. A correlation is developed between the flux sensor data and the CCD camera data so that an accurate measurement of flux distribution can be obtained. In this way enough information of flux distribution on the focal plane can be acquired at each moment of time which allows the study of the plants performance under various conditions. [5] The CCD camera temperature is controlled by a combination of heating and cooling devices. A PID controller regulates the air pressure supplied to a vortex cooler in order to keep the CCD camera temperature constant at 23^{o}C [5]. The heat flux sensors used in the measurement system also require cooling. For accurate heat flux measurement, it is more important to prevent transients in water temperature than to keep a precise set point. Cooling water is supplied from a tank of sufficient thermal mass to prevent any abrupt change in the water temperature and to operate for several hours with less than 20K temperature rise. The water temperature going into the sensors and the outlet temperature of each sensor are recorded and then used in correcting the HFS for thermal losses using a correction model developed in [6, 7]. The foregoing combination of optical and thermal radiometry provide the required flux mapping. While heat flux measurement is accurate and reliable, it is only feasible to be implemented at discrete points on the target. Optical methods on the other hand are less accurate but provide very high spatial resolution. Heat flux measurement is used as a reference for calibrating the optical system and hence combining the advantage of the two methods. Similar hybrid measurement systems have been used to measure heat flux on the targets of parabolic dishes [8] and tower plants [9, 10].

3 Performance Analysis

In this section we present the method used for analyzing the performance of the BDOE. The optical performance of the plant (not including the intercept factor) is evaluated from the experimental results acquired by the flux measurement system. Then the intercept factor and the receiver thermal performance are evaluated simultaneously for varying operating temperatures using the optimization algorithm which is described later in section 3.2.

3.1 Receiver Thermal Performance

Heat loss from solar receivers is a subject of much literature. McDonald [11] presented a comprehensive investigation of heat loss from cavity receivers including convection, radiation and conduction. Receiver convection loss has

been studied in great detail by Clausing [12–14] and others [15–18]. These studies included analytical and numerical models supported by experimental studies for various geometries and receiver orientations. Most of these studies however only considered losses from downward facing receivers except for Leibfried and Ortjohann [15] who also considered upward facing receivers. Although some studies considered forced convection [19], most studies neglected forced convection loss from cavity receivers [12, 15, 16, 18]. In this paper we will base our analysis on the performance of an upward facing open receiver and we will neglect forced convection effects because the mean wind speed during the test was small (2.6 m/s).

Here we present the equations and procedure used in assessing the performance of a hypothetical receiver. The method is based on Hottel-Whillier equation [20] as presented in Duffie and Beckman [21]. The Heat Transfer Fluid (HTF) selected for the analysis is liquid Sodium. Under steady state conditions the net useful power output of the receiver is the difference between the absorbed solar radiation and the thermal loss from the receiver surface.

$$\dot{Q}_u = A(\alpha \dot{Q}_{in} - U_L(T_{mp} - T_e)) \tag{1}$$

Where $\dot{Q}_u$ is the useful heat output, α is the absorptivity of the receiver in the solar spectrum (taken as 95%), $\dot{Q}_{in}$ is the solar power intercepted by the receiver aperture, U_L is the overall heat loss coefficient, T_{mp} is the mean plate temperature and T_e is the air temperature both in K.

Eqn. (1) is reformulated in terms of the inlet fluid temperature (T_{fi}) and the heat removal factor (F_R). F_R is introduced to account for the underestimated losses calculated based on the inlet fluid temperature (T_{fi}) instead of mean plate temperature.

$$\dot{Q}_u = AF_R(\alpha \dot{Q}_{in} - U_L(T_{fi} - T_e)) \tag{2}$$

The heat removal factor F_R reduces the useful gain from what it would have been had the whole absorber plate been at the inlet fluid temperature to what actually occurs [21]. F_R is given by:

$$F_R = \frac{\dot{m}c_p}{AU_L}\left(1 - e^{-\frac{AU_L F'}{\dot{m}C_p}}\right) \tag{3}$$

Where $\dot{m}$ is the mass flow rate, C_p is the specific heat of HTF and F' is the receiver efficiency factor [21] that accounts for the thermal resistance between the plate and the fluid inside the tubes:

$$F' = \frac{1}{U_L D_O\left(\frac{1}{U_L D_i} + \frac{1}{\pi D_i h_f}\right)} \tag{4}$$

Where D_o is the outer tube diameter, D_i is the inner tube diameter and h_f is the convection heat transfer coefficient between the inner wall and the fluid. For liquid metals like liquid sodium, convection heat transfer correlation between the fluid and the tube walls is given by [22]:

$$\begin{array}{ll} Nu_f = 6.3 + 0.0167R_e^{0.85}Pr^{0.93} & Turbulent \\ Nu_f = 4.36 & Laminar \end{array} \tag{5}$$

The overall heat loss coefficient U_L accounts for heat losses in the receiver. There are five main loss mechanisms associated with the receiver of a concentrated solar plant: convective loss, radiative loss, conductive loss, loss due to reflection, and spillage. Conductive heat losses are assumed to be negligible conpared to other loss mechanisms, while losses due to spillage are accounted for in the calculation of intercepted power by the reicever (section 3.2), and reflective losses and spillage around the CR are accounted for by the fact that radiation is measured at receiver aperture level.

According to [23], in a well designed receiver, thermal losses account for 5%-15% of total available energy, hence a reasonable estimate using T_{mp} is adequate to determine receiver performance. We assume, as mentioned earlier, that the dominant convection mode is free convection and that forced convection is negligible. Grashof number for free convection is given by:([22])

$$Gr_L = \frac{\beta \Delta T g L^3}{\nu^2} \tag{6}$$

Where β is the volumetric thermal expansion coefficient in K^{-1},ΔT is the temperature difference between mean plate temperature (T_{mp}) and ambient air temperature (T_e) in K, g is the gravitational acceleration in m/s^2, L is the characteristic length of the receiver equal to it diameter in m, and ν is the kinematic viscosity of air in m^2/s. The Nusselt number for laminar and turbulent flows are given by:([22])

$$\begin{array}{ll} \bar{Nu}_{natural} = 0.54(Gr_L Pr)^{1/4} & ,Turbulent \\ \bar{Nu}_{natural} = 0.14(Gr_L Pr)^{1/3} & ,Laminar \end{array} \tag{7}$$

Therefore, the convection heat transfer coefficient (in W/m^2K) is given by

$$\bar{h}_c = \frac{kNu}{L} \tag{8}$$

Where k is the is the conductivity of air in W/mK. Fluid properties are evaluated at the mean film temperature calculated as $T_{film} = (T_{mp} + T_e)/2$.

The radiative heat loss is given by:

$$\dot{Q}_{rad} = A\varepsilon\sigma(T_{mp}^4 - T_{sky}^4) \tag{9}$$

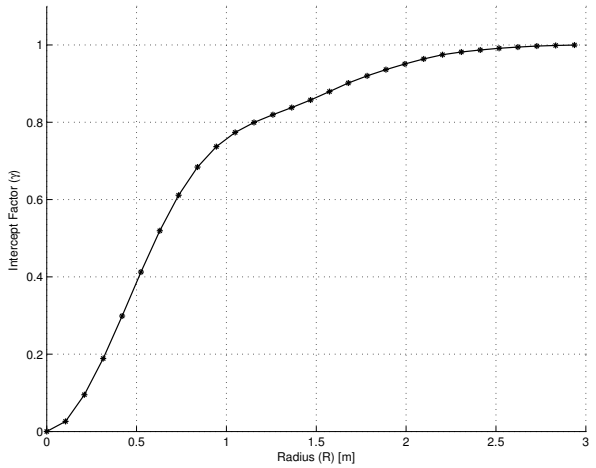

Fig. 2. Day-average intercept factor (γ) as a function of receiver aperture radius (R).

Where $\dot{Q}_{rad}$ is the radiative heat loss in W, $\varepsilon$is the longwave emissivity (taken as 10%),T_{mp} is the mean plate temperature and T_{sky} is the effective sky temperature both in K. Hence the linearized radiative heat transfer coefficient relative to air temperature may be defined as:

$$\bar{h}_r = A\varepsilon\sigma\frac{T_{mp}^4 - T_{sky}^4}{T_{mp} - T_e} \tag{10}$$

The mean plate temperature T_{mp} required for solving the previous equations can be calculated by:

$$T_{mp} = T_{fi} + \frac{Q_u}{AF_RU_L}(1 - F_R) \tag{11}$$

Finally,the overall heat loss coefficient is given by:

$$U_L = \bar{h}_r + \bar{h}_c \tag{12}$$

3.2 Receiver Intercept Factor

Due to various optical and mechanical error sources in the concentration system in addition to sunshape. The power intercepted by the receiver will depend on the receiver aperture size. Fig. 2 depicts the day-average intercept factor variation with receiver aperture radius. The receiver intercept factor γ is calculated as follows:

$$\gamma = \frac{\int_0^R \int_0^{2\pi} G(r,\theta)d\theta dr}{\int_0^\infty \int_0^{2\pi} G(r,\theta)d\theta dr} \tag{13}$$

where γ is the receiver intercept factor, R is the receiver aperture radius, $G(r,\theta)$ is the flux map defined in polar coordinates.

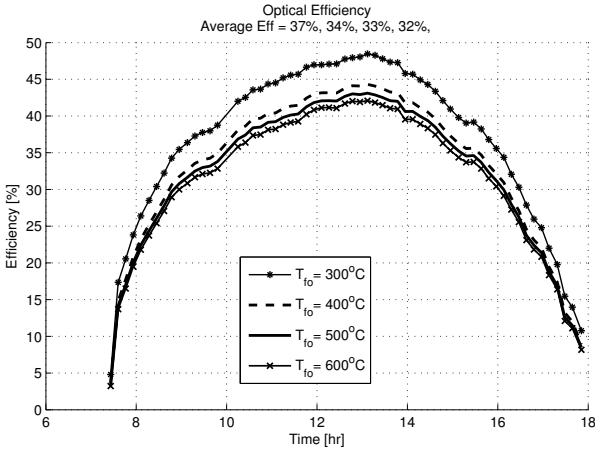

Fig. 3. Optical efficiency with optimal aperture

3.3 Receiver Aperture Sizing

Optimal receiver aperture size is determined by maximizing the day average useful power in Eqn. 2. This is calculated based on the required outlet mean fluid temperature. An iterative algorithm is used for evaluating the receiver performance and finding the optimal receiver size. Depending on the temperature/flow control strategy used, the algorithm is slightly modified. Below is an outline of the major calculation steps used:

1. Calculation of cumulative flux maps which give the relation between receiver size (R) and intercepted power(Q_{in}).
2. Specification of control strategy and setpoint of control variable : mass flow, outlet temperature or optimal outlet temperature.
3. Selection of a receiver radius (R).
4. Calculation of receiver performance based on input paramters : $T_{fi}, T_{fo}, R, Q_{in}$ and ambient conditions.
   (a) Radiation and convection heat transfer coefficients ($\bar{h}_r, \bar{h}_c$) are calculated using an initial value for the mass flow rate ($\dot{m}$) and mean plate temperature (T_{mp}).
   (b) Receiver efficiency factor (F') is calculated.
   (c) $\dot{m}$ is updated using the calculated (F') and overall heat loss coefficient (U_L).
   (d) Net useful power (Q_u) is updated using the new $\dot{m}$ where $Q_u = \dot{m}c_p(T_{fo} - T_{fi})$.
   (e) Heat removal factor (F_R)is updated with the new Q_u.
   (f) T_{mp} is updated.
   (g) Steps a-f are repeated until T_{mp} is accurate enough.
5. The calculation is repeated for different R and T_{fo}.

4 Results

In this section we present the results obtained from the BDOE performance under full concentration using the experimental data collected and the receiver model we presented in previous sections.

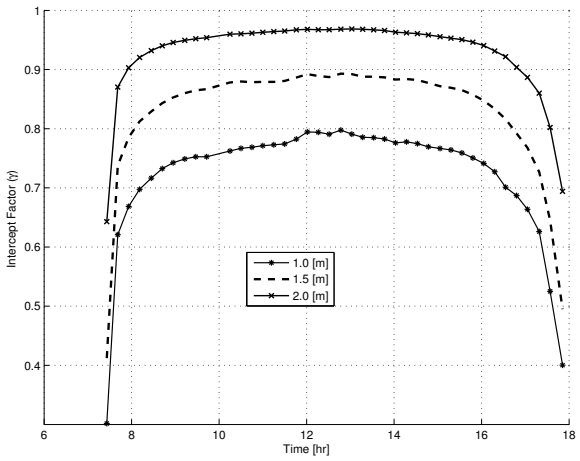

Fig. 4. Intercept factor variation during the day for different receiver aperture sizes

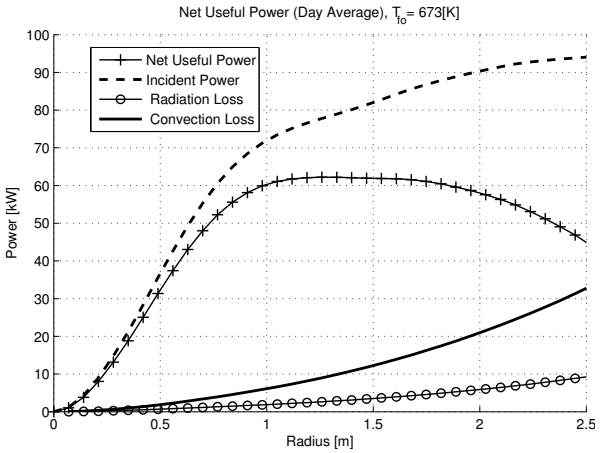

Fig. 6. Net power collected as a function of receiver radius. Convection and radiation losses are also shown as a function of receiver size

4.1 Optical Efficiency

Fig. 3 depicts the optical efficiency calculated based on the optimal receiver size chosen for each fluid outlet temperature. Optical efficiency represents the amount of energy that is intercepted by the receiver aperture normalized by the product of incident DNI and heliostat Area. Optical efficiency accounts for all the factors that reduces the amount of concentrated radiation until it reaches the receiver, but before it gets converted into thermal power.

Optical efficiency includes cosine factor, reflectivity of both heliostats and the CR mirrors, beam attenuation, CR intercept factor (spillage), incident angle modifier, blocking and shading of heliostats,and the intercept factor of the receiver.

In Fig. 3, it can be seen that the average efficiency of the receiver is varying with outlet temperature from 32% to 37%; this is because the optimal receiver size changes based on the required outlet temperature. Since higher temperatures call for smaller receiver apertures, the optical efficiency is degraded. This is directly caused by the lower intercept factor for smaller receiver radii.

Fig. 4 depicts the daily intercept factor variation for different receiver sizes. The daily intercept factor curve is almost flat in the middle region when sun elevation angle is highest but then drops rapidly in early morning and late afternoon. This is mainly caused by optical aberrations (astigmatism in particular) that causes an elongated flux distribution, and therefore results in radiation to be spill outside the receiver aperture. This can be seen more clearly in Fig. 5 which illustrates flux maps taken at three different times of the test day.

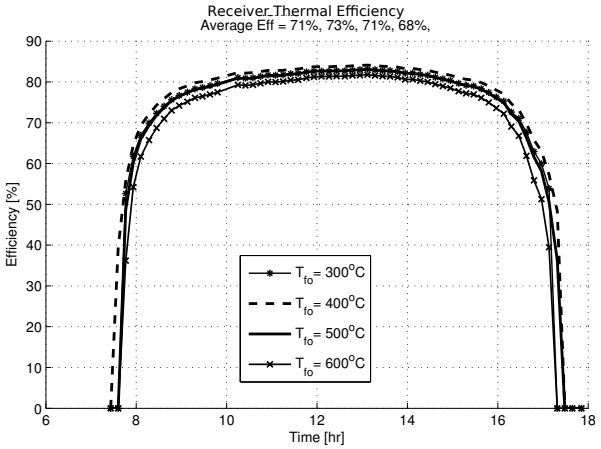

Fig. 7. Receiver thermal efficiency

4.2 Receiver Thermal Efficiency

Receiver thermal efficiency is a function of its mean temperature and aperture size. Fig. 6 illustrates as a function of aperture radius, the incident power on the receiver, convection losses, radiation losses, and net useful output. The curves are calculated for an outlet mean fluid temperature of 400 ^oC. It can be seen that a maxima for net power occurs at a certain receiver radius. Fig. 7 depicts the daily variation of receiver thermal efficiency for several outlet fluid temperatures. It can be seen from Fig. 7 that the receiver thermal efficiency at 400^{o}C (R=1.27 m) is less than that at 500^{o}C (R=1.15 m) or 600^{o}C (R=1.06 m).This is because the optimal receiver aperture size at 400^{o}C is larger, which resulted in a higher thermal losses despite the lower operating temperature. At higher temperatures the effect of thermal losses starts to dominate over the aperture size and we notice that thermal efficiency becomes mainly a function of outlet temperature. It is important to note that since receiver aperture size is optimized for overall efficiency, the overall efficiency at 400^{o}C is still higher than those for higher temperatures.

4.3 Overall Efficiency and Power Output

The overall efficiency (Fig. 8) is the product of optical and thermal efficiencies, as expected it is inversely proportional to the outlet temperature and varying on average from 22% to 26%. Fig. 9 depicts the thermal power output (kW) collected in the HTF for different temperatures. The total energy varies from 623.1 kWh at 400^{o}C to 529.2 kWh at 700^{o}C.

Fig. 10 depicts the maximum possible mechanical power

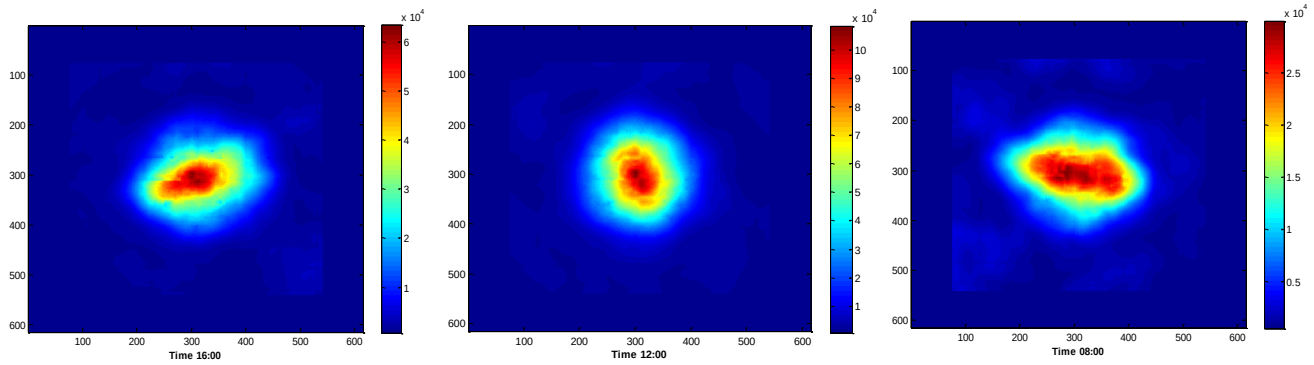

Fig. 5. Flux maps at different times of the day. Aberration is evident in early and late parts of the day which correspond to reduced intercept factor

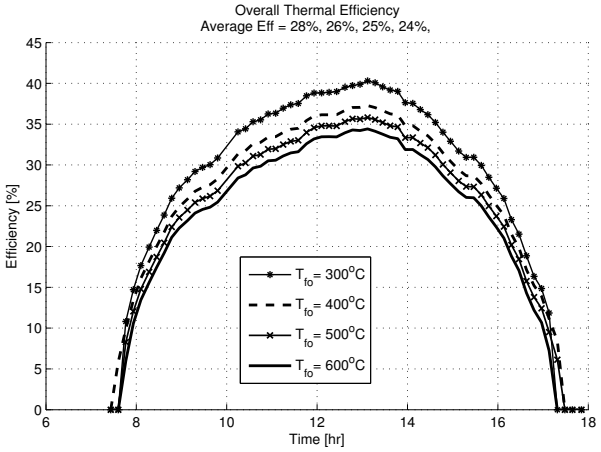

Fig. 8. Overall efficiency

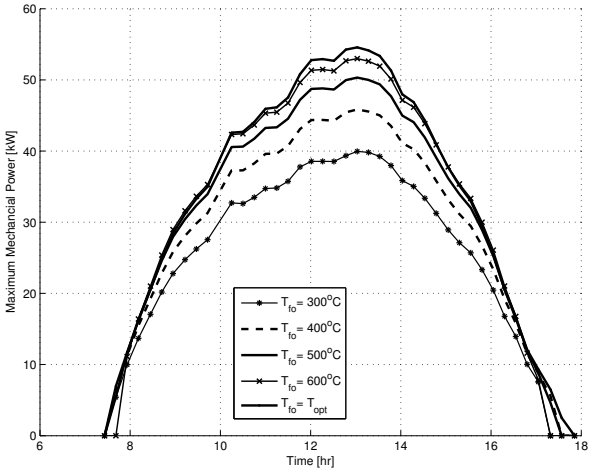

Fig. 10. Maximum Mechanical Power

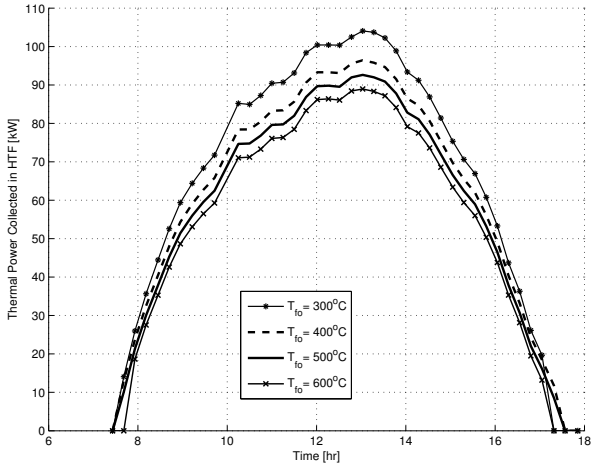

Fig. 9. Thermal output of receiver as function of time and outlet temperature

(exergy rate) of the fluid for varying temperatures, calculated based on Carnot efficiency assuming cold reservoir temperature of 80 ^{o}C. Maximum possible mechanical power is also calculated for real-time optimized fluid outlet temperature ($T_{fo} = T_{opt}$).

4.4 Comparison of Control Strategies

The selection of the control strategy is often dictated by the consumer process, most processes require a constant temperature supply from the heat source. This obvious challenge for solar systems maybe overcome by some kind of thermal inertia (storage) or hybridization with fossil fuel based sources. Therefore the solar engineer might have the choice between constant-temperature-variable-flow control strategy, constant-flow-variable-temperature control strategy or a variable-temperature-variable-flow control strategy that maximizes exergy (or any other objective function).
While constant flow control is the easiest to implement practically because it requires less hardware and also simpler control the merits of the other control strategies might justify the change, this has to be assessed on a system level. The objective function must be modified to include the consumer process operation parameters.

Fig. 11 shows simulation results for the three aforementioned control strategies. It can be seen in (a) that the differences between the three control strategies is negligible. This is because the constant temperature and constant flow rate were also selected by maximizing the objective function.

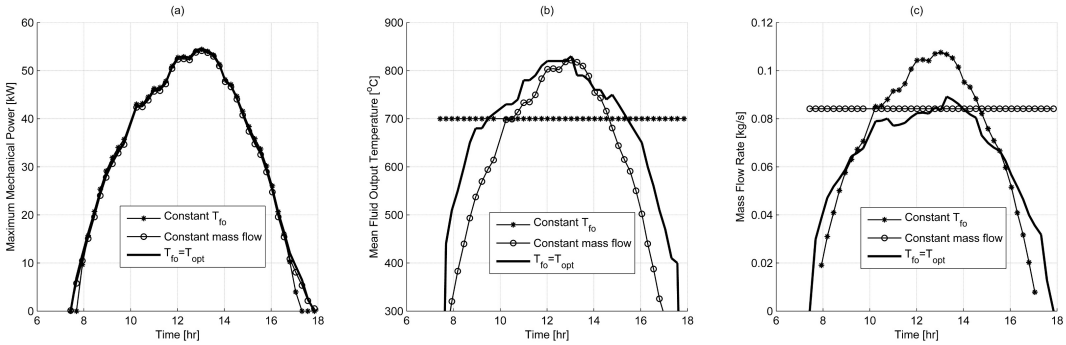

Fig. 11. Comparison of Control Strategies. (a) Daily variation of Maximum Mechanical Power, (b) Mean Fluid Output Temperature, (c) Mass Flow Rate

If the temperature deviates from the optimized constant temperature then the Mechanical Power will be lower (see Fig. 10). It should be also noted that the although the optimal mass flow and outlet temperature are constant in this example day, they are expected to change during the year. Moreover, the small differences between the control strategies are affected by receiver design which have low thermal losses, when thermal losses increase, the real time optimized temperature control strategy may have a significant advantage.

5 Discussion and Conclusions

The overall efficiency of the BDOE varied from 24% to 28% in the test day. The main losses in the system result from optical losses : cosine loss, reflectivity loss, beam attenuation loss, blocking and shading loss in addition to light spillage around Central Reflector (CR) mirrors and around the receiver aperture (intercept factor). The cost incurred by the high optical losses can be justified by the higher temperatures that could be achieved.

References

[1] Kaltschmitt, M., Streicher, W., and Wiese, A., 2007. *Renewable energy : technology, economics and environment*. Springer, New York.

[2] Group, S. . L. L. C. G. . L. L. C., 2003. Assessment of parabolic trough and power tower solar technology cost and performance forecasts. Tech. Rep. NREL/SR-550-34440, Chicago, Illinois, Oct.

[3] Tamaura, Y., Utamura, M., Kaneko, H., Hasuike, H., Domingo, M., and Relloso, S., 2006. "A novel beam-down system for solar power generation with multi-ring central reflectors and molten salt thermal storage". In Proceedings of the 13th International Symposium on Concentrating Solar Power and Chemical Energy Technologies.

[4] Hasuike, H., Yuasa, M., Wada, H., Ezawa, K., Oku, K., Kawaguchi, T., Mori, N., W.Hamakawa, Kaneko, H., and Tamaura, Y., 2009. "Demonstration of tokyo tech beam-down solar concentration power system in 100kw pilot plant". In Proceedings of 15th International Symposium on Concentrated Solar Power and Chemical EnergyTechnologies.

[5] Meyers, S. A., 2011. "Flux mapping of the beam down solar thermal concentrator at masdar city, uae". Master's thesis, Masdar Institute of Science and Technology, Abu Dhabi,UAE.

[6] Mokhtar, M. M., 2011. "The beam-down solar thermal concentrator experimental characterization and modeling". Master's thesis, Masdar Institute of Science and Technology, Abu Dhabi,UAE.

[7] Mokhtar, M. M., Meyers, S. A., Rubalcaba, I., Chiesa, M., and Armstrong, P. R., 2012. "A model for improved solar irradiation measurement at low flux". *Solar Energy,* **86**(3), pp. 837–844.

[8] Ulmer, S., Reinalter, W., Heller, P., Lupfert, E., and Martinez, D., 2002. "Beam characterization and improvement with a flux mapping system for dish concentrators". *Journal of Solar Energy Engineering,* **124**(2), pp. 182–188.

[9] Ballestrín, J., and Monterreal, R., 2004. "Hybrid heat flux measurement system for solar central receiver evaluation". *Energy,* **29**(5–6), pp. 915–924.

[10] Ulmer, S., Lüpfert, E., Pfänder, M., and Buck, R., 2004. "Calibration corrections of solar tower flux density measurements". *Energy,* **29**(5–6), pp. 925–933.

[11] McDonald, C. G., 1995. Heat loss from an open cavity. Tech. Rep. SAND95-2939, Sandia National Labratories.

[12] Clausing, A., 1981. "An analysis of convective losses from cavity solar central receivers". *Solar Energy,* **27**(4), pp. 295–300.

[13] Clausing, A. M., 1983. "Natural convection correlations for vertical surfaces including influences of variable properties". *Journal of Heat Transfer,* **105**(1), pp. 138–143.

[14] Clausing, A. M., Waldvogel, J. M., and Lister, L. D., 1987. "Natural convection from isothermal cubical cavities with a variety of side-facing apertures". *Journal of Heat Transfer,* **109**(2), pp. 407–412.

[15] Leibfried, U., and Ortjohann, J., 1995. "Convective heat loss from upward and downward-facing cavity so-

lar receivers: Measurements and calculations". *Journal of Solar Energy Engineering,* **117**(2), pp. 75–84.

[16] Taumoefolau, T., Paitoonsurikarn, S., Hughes, G., and Lovegrove, K., 2004. "Experimental investigation of natural convection heat loss from a model solar concentrator cavity receiver". *Journal of Solar Energy Engineering,* **126**(2), pp. 801–807.

[17] Prakash, M., Kedare, S., and Nayak, J., 2009. "Investigations on heat losses from a solar cavity receiver". *Solar Energy,* **83**(2), pp. 157–170.

[18] Paitoonsurikarn, S., Lovegrove, K., Hughes, G., and Pye, J., 2011. "Numerical investigation of natural convection loss from cavity receivers in solar dish applications". *Journal of Solar Energy Engineering,* **133**(2), p. 021004.

[19] Ma, R. Y., 1993. Wind effects on convective heat loss from a cavity receiver for a parabolic concentrating solar collector. Tech. Rep. SAND92-7293, Sandia National Labratories.

[20] Hottel, H., and Whillier, A., 1958. "Evaluation of flat-plate solar collector performance". In Transactions of the Conference on Use of Solar Energy (E. F.Carpenter, ed.), University of Arizona Press, p. 74.

[21] Duffie, J. A., and Beckman, W. A., 2006. *Solar engineering of thermal processes*, 3rd edition ed. Wiley.

[22] Mills, A. F., 1998. *Heat Transfer*, 2nd edition ed. Prentice Hall.

[23] Winter, C.-J., Sizmann, R. L., and Vant-Hull, L. L., 1991. *Solar Power Plants: Fundamentals, Technology, Systems, Economics*, first ed. Springer.